NASA
Technical Memorandum 4054

AVSCOM
Technical Memorandum 88-B-013

Predicted and Measured Strain Responses of Isotropic Panels to Base Excitation

Karen H. Lyle, Jack D. Leatherwood,
and Edward F. Daniels

AUGUST 1988

NASA

US ARMY
AVIATION
SYSTEMS COMMAND
AVIATION R&T ACTIVITY

NASA
Technical Memorandum 4054

AVSCOM
Technical Memorandum 88-B-013

Predicted and Measured Strain Responses of Isotropic Panels to Base Excitation

Karen H. Lyle
Aerostructures Directorate
USAARTA-AVSCOM
Langley Research Center
Hampton, Virginia

Jack D. Leatherwood and Edward F. Daniels
Langley Research Center
Hampton, Virginia

National Aeronautics
and Space Administration

Scientific and Technical
Information Division

1988

Summary

The objective of the research described is to assess the accuracy of classical linear theory for predicting acceleration and strain for cantilevered and clamped-free-clamped-free (C-F-C-F) panels excited through the base. Aluminum, stainless steel, and titanium panels of various dimensions and thicknesses were vibration tested by using a broadband random signal applied through a shaker mounting fixture. The strains were measured at nine locations on each cantilevered panel and at five locations on each C-F-C-F panel. Accelerations were measured on the base and at one panel location for both the cantilevered and the C-F-C-F panels. Predictions were based on the Ritz method with assumed beam functions. The measured accelerations of the base and modal damping values were input to the analysis. Measured and predicted modal frequencies agree to within 4 percent. Comparisons between predicted and measured strain and acceleration spectra were within an average error of 20 percent for both the cantilevered and the C-F-C-F panels.

Introduction

An analytical and experimental research program has been initiated at the NASA Langley Research Center to investigate the strain response of panels under severe thermal and/or acoustic loads. The ultimate goal of the program is to develop methods for predicting panel stresses and strains that may lead to improved understanding of sonic fatigue failure in advanced aircraft (high sound levels on aluminum, composite, and sandwich panels) and in advanced aerospace vehicles (high temperature and high sound levels on sandwich panels). The initial research, described herein, focuses on flat, rectangular, isotropic panels at ambient temperatures.

Many acoustic-response research studies have been conducted on conventional aluminum panels, and the resulting large base of experimental data has enabled good empirical understanding and confident sonic fatigue design methods (refs. 1 to 9). More recently there has been similar research with composite and sandwich panels to develop empirical sonic fatigue methods (refs. 10 to 14); however, complications in predicting the structural response have caused the design methods for composite and sandwich panels to be much less reliable than those for aluminum panels. These complications include poorly predicted natural frequencies, nonlinear large deflections, and frame and panel boundary problems. Because sandwich and composite panels can be made with a great variety of structural properties, a reliable analytical model is highly desirable to reduce the effort and costs associated with the large amount of test data needed in developing empirical design charts similar to those that already exist for aluminum panels.

Unfortunately, poor comparisons between measured and predicted bending and membrane strains have occurred in the composite- and sandwich-panel research programs that are due not only to the structural modeling complexities but also to complications in noise spatial distribution and frequency spectrum. These complications include complex incident sound waves (i.e., neither plane waves nor grazing waves) and frequency spectra varying greatly over the frequency range of interest. Although the predictions of natural frequencies and deflections compare very well with measurements and the predominance of the fundamental mode can be established, the predictions of bending strain can differ from measurements by a factor of 2 or more (refs. 11 and 13).

Because of these past difficulties in obtaining agreement between measured and predicted strains, a program assessing the accuracy of classical linear theory for predicting strain was initiated in a controlled environment. The dynamic structural excitation was restricted to low levels so that the use of small deflection theory was applicable in the analysis.

The present paper presents the initial results of this work. The first section describes the experimental portion of the research, including detailed descriptions of the panel mounting fixture, the test panels, and the data analysis. The next section describes the analytical model which applies the Ritz method with base excitation to cantilevered and clamped-free-clamped-free

(C-F-C-F) panels. These sections are followed by the comparison of experimental and analytical results. The final section summarizes the current status of the research.

Symbols

A_a	base acceleration, in/sec^2
A_w	base displacement, in.
A_{ij}^k	eigenvector for kth eigenvalue
a	panel length, in.
$\bar{B}_k$	kth complex mode shape coefficient, in.
b	panel width, in.
D	bending stiffness, $Eh^3/[12(1-\mu^2)]$, in-lb
E	Young's modulus, lb/in^2
F	displacement function for panel
f	frequency, Hz
h	panel thickness, in.
p	panel loading, lb
Q	work energy, in-lb
q	forced excitation, lb/in^2
T	kinetic energy, in-lb
t	time, sec
U	displacement of base, in.
V	potential energy, in-lb
W	panel displacement for pseudouniform pressure excitation, in.
w	panel displacement, in.
x	distance along panel length, in.
y	distance along panel width, in.
Z_k	kth mode shape
α_m, β_m	coefficients in cantilevered/clamped-clamped beam function
γ_n, δ_n	coefficients in free-free beam function
ϵ_x	strain parallel to x-axis (longitudinal), in/in.
ϵ_y	strain parallel to y-axis (lateral), in/in.
ς	percent of critical damping
λ_k	kth eigenvalue
μ	Poisson's ratio
ρ	mass density, lb-sec^2/in^4
ϕ_m	mth cantilevered/clamped-clamped mode shape

ψ_n nth free-free mode shape

Abbreviation:

FFT fast Fourier transform

Notation:

$\ddot{\cdot}$ $= \partial^2/\partial t^2$

∇ del operator

Partial derivatives with respect to x and y variables are shown as subscripts following a comma; e.g., $F_{,x} = \partial F/\partial x$.

Description of Experiment

The responses of cantilevered and clamped-free-clamped-free (C-F-C-F) rectangular, isotropic panels subjected to base excitation applied at the clamped ends were experimentally determined in this investigation. A photograph showing the apparatus used to study panel response for cantilevered panels is shown in figure 1. Sketches of the cantilevered and clamped-free-clamped-free (C-F-C-F) test apparatus are shown in figure 2. Cantilevered boundary conditions were achieved by placing the panels between two clamping blocks as shown in figures 1 and 2(a). To obtain as near a clamped condition as possible, it was necessary to place lead inserts between the upper and lower panel surfaces and the clamping devices (blocks). These lead inserts, approximately 1/8 in. thick, provided high damping at the clamped end and tended to fill voids along the clamped boundary surfaces. The upper clamping block was attached to the lower clamping block by a series of bolts extending through the lead inserts and test specimen. The lower clamping block was bolted directly to the moving shaker head. Clamping pressure on the test panels was generated by applying torque to the bolts connecting the upper and lower clamping blocks. Considerable effort was devoted to obtaining clamped boundaries, and the above method provided the most consistent and repeatable results for the cantilevered panels.

The C-F-C-F boundary conditions proved to be more difficult to obtain experimentally because attempts to clamp opposite ends of the test panels introduced mechanical loads and prestresses that modified the stiffness characteristics of the panels. This was due to factors such as misalignment of the opposing clamping devices, initial panel curvatures, and local panel irregularities at the clamping surfaces. To minimize the problem of mechanically induced preloads, the clamping method illustrated in figure 2(b) was used. This method utilized an aluminum support fixture containing a fixed clamping device at one end and a movable clamping device at the other end. The movable clamping device provided vertical and rotational adjustment capability for alleviating the preloads. This was accomplished by observing selected panel strain gauge outputs while performing clamping adjustments at the movable end. It should be noted, however, that it was not possible to obtain conditions for which the panels were totally free of preloads, particularly in the y-axis (lateral) direction.

Eight cantilevered and three C-F-C-F thin, metallic, rectangular panels were tested in this investigation. The panels, made of aluminum, stainless steel, and titanium, were milled from available sheet stock and no attempt was made to impose strict dimensional tolerances. The material properties, measured dimensions, and transducer locations for each panel are given in table I, with the key to the dimensions given in figure 3. For each cantilevered panel, total surface strains were measured at nine locations. Only data obtained at locations 2, 3, 5, and 6 are presented in this paper. Data from five surface-strain locations were obtained for the C-F-C-F panels, but only sample data at location 1 are presented. Accelerations were measured at one location on each panel as well as at the base. However, only acceleration data for panel 2 are presented. The data selected for presentation are typical of those obtained at the remaining locations.

A diagram of the instrumentation setup is presented in figure 4. A selected base excitation was applied to the clamping fixture using an electromagnetic shaker having a rated force of 100 lb (peak sine wave), a dynamic stroke of 0.75 in. (peak to peak), and a rated velocity of 100 in/sec. The useful frequency range of the shaker was dc (direct current) to 6500 Hz. Random base (shaker head) acceleration having approximately uniform spectral density over the frequency range from 50 to 600 Hz was obtained by band pass filtering and equalization of the output of a random-noise generator. Equalization was necessary in order to compensate for roll-off of shaker performance with increasing frequency. The equalizer output was applied to a power amplifier whose output voltage signal provided the drive signal to the shaker armature. A sample base acceleration obtained from an accelerometer attached to the upper clamping block is shown in figure 5 for cantilevered panel 4. (Acceleration is given in g units where $1g \approx 32.174$ ft/sec^2.)

Analog outputs from each sensor were applied to a digital processing system for spectrum and time series analysis, identification of modal characteristics, and signal storage. Each of the measured panel response signals was analyzed to determine spectral characteristics of panel strain and acceleration response, panel-acceleration to base-acceleration transfer functions, and panel strain to base-acceleration transfer functions. A standard circle-fit procedure (ref. 15) was also applied to identify the modal frequency and damping characteristics of the observed response modes. The results of these analyses were used for comparison with theoretical narrow band predictions of panel strain and acceleration response.

Analysis

The prediction model for both the cantilevered and the C-F-C-F panels is based on the Ritz method. In each case, for the clamped boundaries, the model assumes no translational or rotational motion of the panel relative to the clamping surface; and for the free boundaries, the moment and shear force are zero.

For an isotropic, rectangular panel the equation of motion is given as (ref. 16)

$$D\,\nabla^4\,w(x,y,t) + \rho h\,\ddot{w}(x,y,t) = p(x,y,t) \tag{1}$$

where D is the bending stiffness, ρ is the panel density, h is the panel thickness, $p(x,y,t)$ is the external panel loading, and $w(x,y,t)$ is the panel displacement. In the case of a moving base with no external loads, then $p(x,y,t) = 0$. For harmonic motion, where

$$w(x,y,t) = w(x,y)\,e^{i2\pi ft}$$

then equation (1) becomes

$$D\,\nabla^4\,w(x,y) - 4\pi^2\rho h f^2\,w(x,y) = 0 \tag{2}$$

where f is the frequency. The boundary conditions for the cantilevered panel, where the base displacement is A_w, are given as

$$\left.\begin{aligned} &w(0,y) = A_w \\ &w_{,x}\,(0,y) = w_{,xx}\,(a,y) = w_{,xxx}\,(a,y) = 0 \\ &w_{,yy}\,(x,0) = w_{,yyy}\,(x,0) = w_{,yy}\,(x,b) = w_{,yyy}\,(x,b) = 0 \end{aligned}\right\} \tag{3a}$$

The boundary conditions for a C-F-C-F panel are the same as those for a cantilevered panel except along the $x = a$ edge, where the conditions are described by

$$w(a,y) = A_w \qquad \text{and} \qquad w_{,x}\,(a,y) = 0 \tag{3b}$$

Using the transformation (ref. 17)

$$w(x,y) = W(x,y) + U(x,y) \tag{4}$$

where $W(x,y)$ and $U(x,y)$ are components of panel displacement, and substituting into equation (2) yields

$$D\ \nabla^4\ W(x,y) - 4\pi^2\rho h f^2\ W(x,y) = -D\ \nabla^4\ U(x,y) + 4\pi^2\rho h f^2\ U(x,y) \tag{5}$$

The displacement $W(x,y)$ can be solved for classical cantilevered boundary conditions for an excitation given by the right-hand side of equation (5). The panel displacement $U(x,y)$ must satisfy the following conditions:

$$\left.\begin{aligned}
&W(0,y) = A_w - U(0,y)\\
&W_{,x}\,(0,y) = 0 - U_{,x}\,(0,y) = -U_{,x}(0,y)\\
&W_{,xx}\,(a,y) = 0 - U_{,xx}\,(a,y) = -U_{,xx}(a,y)\\
&W_{,xxx}\,(a,y) = 0 - U_{,xxx}\,(a,y) = -U_{,xxx}(a,y)\\
&W_{,yy}\,(x,0) = 0 - U_{,yy}\,(x,0) = -U_{,yy}(x,0)\\
&W_{,yyy}\,(x,0) = 0 - U_{,yyy}\,(x,0) = -U_{,yyy}(x,0)\\
&W_{,yy}\,(x,b) = 0 - U_{,yy}\,(x,b) = -U_{,yy}(x,b)\\
&W_{,yyy}\,(x,b) = 0 - U_{,yyy}\,(x,b) = -U_{,yyy}(x,b)
\end{aligned}\right\} \tag{6a}$$

For the C-F-C-F panels, the conditions at $x = a$ are

$$\left.\begin{aligned}
&W(a,y) = A_w - U(a,y)\\
&W_{,x}\,(a,y) = 0 - U_{,x}\,(a,y) = -U_{,x}(a,y)
\end{aligned}\right\} \tag{6b}$$

For either case, for this experiment the function $U(x,y)$ is

$$U = \text{Constant} = A_w \tag{7}$$

which would make the right-hand sides of all parts of equation 6 equal to zero. Substitution of U into equation (5) gives

$$D\ \nabla^4\ W(x,y) - 4\pi^2\rho h f^2\ W(x,y) = 4\pi^2\rho h f^2 A_w \tag{8}$$

The response $W(x,y)$ is calculated by the Ritz method which is based on minimizing the following conservation of energy equation:

$$T - (V + Q) = \text{Constant} \tag{9}$$

where T is the kinetic energy, V is the potential energy, and Q is the work energy. For a rectangular, isotropic panel the potential energy in bending is given by (ref. 18)

$$V = \frac{D}{2}\int_0^a\int_0^b \left([F_{,xx}\,(x,y) + F_{,yy}\,(x,y)]^2 - 2(1-\mu)\left\{ F_{,xx}\,(x,y)\ F_{,yy}\,(x,y) - [F_{,xy}\,(x,y)]^2 \right\} \right) dx\ dy \tag{10}$$

the kinetic energy is given by

$$T = 2\pi^2\rho h f^2 \int_0^a\int_0^b F^2(x,y)\ dx\ dy \tag{11}$$

and the work energy is given by

$$Q = \int_0^a \int_0^b F(x,y)\, q(x,y)\, dx\, dy \tag{12}$$

where $F(x,y)$ is the displacement function for the panel and $q(x,y)$ is the panel loading.

The forced displacement response of the panel is given by the following summation of mode shapes:

$$W(x,y) = \sum_{k=1}^{r} \bar{B}_k\, Z_k(x,y) \tag{13}$$

where $\bar{B}_k$ is a complex coefficient, and for each mode the mode shape is given by

$$Z_k(x,y) = \sum_{m=1}^{p} \sum_{n=1}^{q} A_{mn}^k\, \phi_m(x)\, \psi_n(y) \tag{14}$$

The displacement functions $\phi_m(x)$ and $\psi_n(y)$ are assumed beam modes (ref. 18), where in the x-direction

$$\phi_m(x) = \cosh(\beta_m x/a) - \cos(\beta_m x/a) - \alpha_m[\sinh(\beta_m x/a) - \sin(\beta_m x/a)] \tag{15a}$$

and in the y-direction

$$\left.\begin{aligned} &\psi_1 = 1 \\ &\psi_2(y) = \sqrt{3}\,[1 - (2y/b)] \\ &\psi_n(y) = \cosh(\gamma_n y/b) + \cos(\gamma_n y/b) - \delta_n[\sinh(\gamma_n y/b) + \sin(\gamma_n y/b)] \qquad (n \geq 3) \end{aligned}\right\} \tag{15b}$$

The reader should note that the different boundary conditions for the cantilevered and the C-F-C-F panels in the x-direction result in different numerical values for β_m and α_m in equation (15a). The values for α_m, β_m, δ_n, and γ_n are calculated in reference 19.

The eigenvalues λ_k and eigenvectors A_{ij}^k are calculated from the free-vibration response, i.e., $Q = 0$ in equation (9). Minimizing the conservation of energy expression, where $F(x,y) = Z_k(x,y)$, with respect to A_{ij}^k results in the standard eigenvalue problem of the form

$$([\mathbf{X}] - \lambda[\mathbf{I}])\{\mathbf{A}\} = 0 \tag{16}$$

where $[\mathbf{I}]$ is the identity matrix and the matrix $[\mathbf{X}]$ and the vector $\{\mathbf{A}\}$ are determined from

$$\frac{\partial T}{\partial A_{ij}^k} - \frac{\partial V}{\partial A_{ij}^k} = 0 \tag{17}$$

The solution of the matrix in equation (16) for the eigenvalues and eigenvectors will lead to the natural frequencies and mode shapes. Numerical values for the eigenvalues and eigenvectors are given in reference 18. The natural frequency f_k is related to the eigenvalue by

$$f_k = \frac{1}{2\pi}\left(\frac{\lambda_k D}{\rho h a^4}\right)^{1/2} \tag{18}$$

Returning to the forced solution and minimizing the conservation of energy expression, where $F(x,y) = W(x,y)$, with respect to $\bar{B}_k$ yields

$$\frac{\partial T}{\partial \bar{B}_k}\left[\left(\frac{f_k}{f}\right)^2 - 1\right] = \frac{\partial Q}{\partial \bar{B}_k} \tag{19}$$

since

$$\frac{\partial V}{\partial \bar{B}_k} = 4\pi^2 \frac{\partial T}{\partial \bar{B}_k}$$

The loading on the plate is given by

$$q(x,y) = 4\pi^2 \rho h f^2 A_w \tag{20}$$

Thus, the work energy Q is

$$Q = 4\pi^2 \rho h f^2 A_w \int_0^a \int_0^b W(x,y)\, dx\, dy \tag{21}$$

Solving equation (19) for $\{\bar{\mathbf{B}}\}$ yields

$$\bar{B}_k = \frac{2A_w f^2 \sum_{m=1}^{q} (A_{m1}^k \alpha_m/\beta_m)}{f_k^2 - f^2} \qquad \text{(undamped)} \tag{22}$$

where A_w is frequency dependent. For small damping values, the percent of critical damping ς can be included by the addition of $2i\varsigma f f_k$ to the denominator of equation (22):

$$\bar{B}_k = \frac{2A_w f^2 \sum_{m=1}^{q} (A_{m1}^k \alpha_m/\beta_m)}{f_k^2 + 2i\varsigma f f_k - f^2} \qquad \text{(damped)} \tag{23a}$$

where $i = \sqrt{-1}$. Since the excitation is customarily measured as base acceleration A_a, where $A_a = 4\pi^2 f^2 A_w$, then

$$\bar{B}_k = \frac{2A_a \sum_{m=1}^{q} (A_{m1}^k \alpha_m/\beta_m)}{4\pi^2(f_k^2 + 2i\varsigma f f_k - f^2)} \qquad \text{(damped)} \tag{23b}$$

Thus, $\bar{B}_k$ can now be substituted into equation (13).

The strain is calculated from the displacement in the x-direction, by

$$\epsilon_x = -\frac{h}{2}\frac{\partial^2 w(x,y)}{\partial x^2} \tag{24}$$

and in the y-direction by

$$\epsilon_y = -\frac{h}{2}\frac{\partial^2 w(x,y)}{\partial y^2} \tag{25}$$

The acceleration is given by

$$\ddot{w}(x,y) = -4\pi^2 f^2\ w(x,y) = -4\pi^2 f^2[W(x,y) + A_w] \tag{26}$$

The root-mean-square (rms) spectral values in the x-direction are defined for rms excitation to be

$$\epsilon_{x,\mathrm{rms}}(f) = (\epsilon_x \epsilon_x^*)^{1/2} \tag{27}$$

where the superscript * denotes the complex conjugate. Thus, substitution of equation (24) into (27) gives

$$\epsilon_{x,\mathrm{rms}}(f) = \frac{h}{2}\left\{ \frac{\partial^2}{\partial x^2}\left[\sum_{k=1}^{r}(\bar{B}_k)_{\mathrm{real}}\ Z_k\right]^2 + \frac{\partial^2}{\partial x^2}\left[\sum_{k=1}^{r}(\bar{B}_k)_{\mathrm{imag}}\ Z_k\right]^2 \right\}^{1/2} \tag{28}$$

where the subscripts real and imag refer to the real and imaginary parts, respectively, of the quantity in parentheses. Likewise, it can be shown that

$$\epsilon_{y,\mathrm{rms}}(f) = \frac{h}{2}\left\{ \frac{\partial^2}{\partial y^2}\left[\sum_{k=1}^{r}(\bar{B}_k)_{\mathrm{real}}\ Z_k\right]^2 + \frac{\partial^2}{\partial y^2}\left[\sum_{k=1}^{r}(\bar{B}_k)_{\mathrm{imag}}\ Z_k\right]^2 \right\}^{1/2} \tag{29}$$

and

$$\ddot{w}_{\mathrm{rms}}(f) = 4\pi^2 f^2\left\{ \left[\sum_{k=1}^{r}(\bar{B}_k)_{\mathrm{real}}\ Z_k + (A_w)\right]^2 + \left[\sum_{k=1}^{r}(\bar{B}_k)_{\mathrm{imag}}\ Z_k\right]^2 \right\}^{1/2} \tag{30}$$

Finally, the overall (denoted by the subscript oa) rms strains and accelerations over the frequency range from 25 to 500 Hz were calculated by

$$\left.\begin{aligned} \epsilon_{x,\mathrm{oa}} &= \left[\sum_{f=25}^{500} \epsilon_{x,\mathrm{rms}}^2(f)\right]^{1/2} \\ \epsilon_{y,\mathrm{oa}} &= \left[\sum_{f=25}^{500} \epsilon_{y,\mathrm{rms}}^2(f)\right]^{1/2} \\ \ddot{w}_{\mathrm{oa}} &= \left[\sum_{f=25}^{500} \ddot{w}_{\mathrm{rms}}^2(f)\right]^{1/2} \end{aligned}\right\} \tag{31}$$

Results and Discussion

For each panel, the measured and predicted strain spectra were compared for a frequency resolution of 1 Hz. As shown in figure 6, the measured results for cantilevered panel 4 verify that the panels vibrated in the linear-response region so that a linear analytical model was justified. Each panel was tested at three excitation levels and showed similar linearity results. The highest excitation level was chosen for the comparisons, since it provided the best signal-to-noise ratio in the experimental results. Measured and predicted natural frequencies and overall rms strains are presented in figures 7 and 8. Panel geometry, material properties, and transducer locations are described in table I. Figure 3 shows the transducer locations.

The comparisons for measured and predicted natural frequencies are presented in figure 7. Included in the figure is a table of the measured natural frequencies and damping values. The damping values indicate that the test panels were lightly damped. The unusually high damping value for the second mode of cantilevered panel 3 has not been explained; however, this mode is still considered to be lightly damped. The agreement between the measured and predicted frequency values is within 5 percent, with the cantilevered and C-F-C-F panel natural frequencies predicted equally well. The small discrepancies may be attributed to variances in panel material properties and the inability to obtain perfectly clamped edges.

The comparisons between experimental and analytical overall rms strain values are shown in figure 8. Overall rms strain is the total strain at a point due to the integrated effect of all spectral strain components, as calculated in equation (8). The lines on the figure denote the ±50-percent and ±100-percent accuracy boundaries where accuracy is defined as the percent of deviation of predicted values from the measured values. It is observed that most of the points fall within the 50-percent boundaries with the exception of the data for cantilevered panel 5 (denoted by $\oplus$) and the transverse (y-axis) strain for the C-F-C-F panel (denoted by $\boxplus$).

The source of error in the predictions of overall strain level for panel 5 is not clear. It may, however, be related to a possible coupling of panel response with the base motion. This coupling is illustrated in figure 9 which shows a sharp peak and dip in base acceleration at frequencies close, but not identical, to the fundamental frequency of panel 5. Use of this base-acceleration spectrum as input to the analytical model could have contributed to the large difference between measured and predicted strains. The source of this coupling could not be determined although it did occur for another panel, panel 7, made of the same material and, like panel 5, was one of the heavier panels tested. The discrepancies between measured and predicted transverse strains for the C-F-C-F panels probably resulted from changes in panel curvature and/or mechanical preloads induced by the adjustable clamping device. Although the longitudinal (x-axis) strains could be approximately nulled by adjustments of the clamping mechanism, it was not possible to set the transverse strains to zero simultaneously. In fact, generally the lateral (y-axis) static strains significantly increased as the x-axis strains were minimized during adjustment. This resulted in preloads that likely affected panel stiffness properties and significantly influenced y-axis strain response, particularly at resonance.

If the y-strain measurements for the C-F-C-F panels are omitted because of their questionable accuracy, then the data of figure 8 would indicate that the average difference between measured and predicted overall rms strains is approximately 20 percent. This agreement is felt to be very good, particularly in light of the uncertainties in experimentally derived damping values and the inability to achieve perfectly clamped boundary conditions.

Measured and predicted strain spectra for location 2 on panel 4 are shown in figure 10. Location 2 was nearest the theoretical highest strain location on the cantilevered panel, i.e., perpendicular to the middle of the clamped edge. In addition, the strains in the y-direction were measured and predicted, as shown in figure 11 for location 5 on panel 4. The y-direction strain in these panels was the lowest since the panels behave much like cantilevered beams with very little bending across the panel width. In both figures 10 and 11, the experimental and analytical strain spectra compare well in both magnitude and shape over the entire frequency range. The higher mode resonant peaks do not match exactly, but this deviation is to be expected because of the added stiffness effect of the Ritz method. All modes in the x-direction are excited because of unsymmetric boundary conditions, i.e., clamped and free. However, the base motion excites the panel like a uniform pressure, so only modes of odd half-wavelengths in the y-direction appear. Thus, the second panel mode is not excited. The differences in measured and predicted panel responses of the resonant peaks are not unexpected. It is generally difficult to predict peaks accurately that are proportional to the damping values used in the analysis. The slight differences between predicted and measured modal frequencies for the fundamental cantilevered modes are attributed to imperfections in the test panels and inexact panel clamping.

Figure 12 shows typical predicted and measured strain results for a C-F-C-F panel, location 1 on panel 1. In this case the model also predicts the magnitude and shape of the measured strain spectra accurately. Since the panel has nearly symmetric boundary conditions in the x-direction, only the first mode is excited in the frequency range investigated, i.e., from 25 to 500 Hz. Any nonsymmetry in the x-direction is due to panel imperfections and inexact clamping at the panel edges. The additional restraints of the second clamped edge cause a higher fundamental frequency for the C-F-C-F panels than for the cantilevered panels. However, like the cantilevered panels, the discrepancy in the magnitude of the response at the fundamental frequency may be attributed to inaccurate modal damping measurements.

The panel accelerations, unlike the strains, depend directly on the acceleration of the base. (See eq. (19).) Hence, it was important in the analysis to incorporate base effects and phase information correctly. A typical example of the ability of the analytical model to predict panel acceleration response is shown in figure 13 for panel 2. It is seen that the analysis was able to predict both the resonant and antiresonant response characteristics of the panel. These results, together with the strain-response results, illustrate the capability of the model to predict accurately both strain response and acceleration response at any specified location on the surface of an isotropic panel.

Concluding Remarks

To date, much work has been done in evaluating the accuracy of a linear isotropic response theory for plate deflection as well as modal frequencies and mode shapes. However, little, if any, work appears to have assessed the accuracy, or even applicability, of such linear theory toward predicting strains. In conclusion, this paper shows that the Ritz method, using assumed beam functions, predicted the linear strain and linear acceleration response spectra of isotropic panels with an accuracy of approximately 20 percent. The discrepancies between predicted and measured results are likely due to uncertainties in the experimentally determined damping values and the inability to obtain ideal clamped boundary conditions. In addition, the analysis was effective in predicting the detailed spectrum characteristics of panel response as well as the variations in response across the panel surfaces. Having verified the linear-strain prediction theory, the research program can more confidently progress to predicting more complicated effects, such as nonlinear panel response and elevated temperatures on strain response.

NASA Langley Research Center
Hampton, Virginia 23665-5225
June 24, 1988

References

1. Lassiter, Leslie W.; and Hess, Robert W.: *Calculated and Measured Stresses in Simple Panels Subject to Intense Random Acoustic Loading Including the Near Noise Field of a Turbojet Engine.* NACA Rep. 1367, 1958. (Supersedes NACA TN 4076.)
2. Clarkson, B. L.; and Ford, R. D.: The Response of a Typical Aircraft Structure to Jet Noise. *J. Royal Aeronaut. Soc.*, vol. 66, Jan. 1962, pp. 31–40.
3. Douglas Aircraft Co., Inc.: *Structural Design for Acoustic Fatigue.* ASD-TDR-63-820, U.S. Air Force, Oct. 1963.
4. Schneider, C. W.: *Development of an Empirical Method for Calculating Dynamic Stresses in Flat Elastic Panels.* ER-9702, Lockheed-Georgia Co., Dec. 29, 1967.
5. Ballentine, John R.; Rudder, Fred F., Jr.; Mathis, James T.; and Plumblee, Harry E., Jr.: *Refinement of Sonic Fatigue Structural Design Criteria.* AFFDL-TR-67-156, U.S. Air Force, Jan. 1968. (Available from DTIC as AD 831 118.)
6. Clarkson, B. L.: Stresses in Skin Panels Subjected to Random Acoustic Loading. *Aeronaut. J.*, vol. 72, no. 695, Nov. 1968, pp. 1000–1010.
7. Thompson, A. G. R.; and Lambert, R. F.: *Acoustic Fatigue Design Data, Part II.* AGARD-AG-162-Pt. II, Nov. 1972.

8. Rudder, F. F., Jr.; and Plumblee, H. E., Jr.: *Sonic Fatigue Design Guide for Military Aircraft.* AFFDL-TR-74-112, U.S. Air Force, May 1975. (Available from DTIC as AD B004 600L.)
9. Jacobson, Marcus J.: *Sonic Fatigue Design Data for Bonded Aluminum Aircraft Structures.* AFFDL-TR-77-45, U.S. Air Force, June 1977. (Available from DTIC as AD B020 118L.)
10. Jacobson, Marcus J.: *Advanced Composite Joints Design and Acoustic Fatigue Characteristics.* AFFDL-TR-71-126, U.S. Air Force, July 1971. (Available from DTIC as AD 890 037L.)
11. Wright, G. C.: *Dynamic Behaviour of Fibre Reinforced Plastic Beams and Plates.* Ph.D. Thesis, Univ. of Southampton, May 1973.
12. Holehouse, Ian: *Sonic Fatigue Design Techniques for Advanced Composite Aircraft Structures.* AFWAL-TR-80-3019, U.S. Air Force, Apr. 1980. (Available from DTIC as AD A090 553.)
13. Teh, Chin Eng: *Dynamic Behaviour and Acoustic Fatigue of Isotropic and Anisotropic Panels Under Combined Acoustic Excitation and Static In-Plane Compression.* Ph.D. Thesis, Univ. of Southampton, Aug. 1981.
14. Holehouse, Ian: *Sonic Fatigue Design Techniques for Advanced Composite Airplane Structures.* Ph.D. Thesis, Univ. of Southampton, 1984.
15. Ewins, D. J.: *Modal Testing: Theory and Practice.* John Wiley & Sons Inc., c.1984.
16. Ashton, J. E.; and Whitney, J. M.: Theory of Laminated Plates. *Progress in Materials Science Series, Volume IV,* Technomic Publ. Co., Inc., c.1970.
17. Myint-U, Tyn: *Partial Differential Equations of Mathematical Physics, Second ed.* Elsevier Science Publ. Co., Inc., c.1980.
18. Young, Dana: Vibration of Rectangular Plates by the Ritz Method. *J. Appl. Mech.*, vol. 17, no. 4, Dec. 1950, pp. 448–453.
19. Young, Dana; and Felgar, Robert P., Jr.: *Tables of Characteristic Functions Representing Normal Modes of Vibration of a Beam.* Publ. No. 4913, Eng. Res. Ser. No. 44, Bureau of Engineering Research, Univ. of Texas, July 1, 1949.

Table I. Panel Material Properties, Dimensions, and Transducer Locations

[The symbols c, d, e_n, g, and g_n refer to transducer locations shown in fig. 3]

(a) Cantilevered panels (see fig. 3(a))

Panel	Material	a, in.	b, in.	c, in.	d, in.	e_1, in.	e_2, in.	e_3, in.	e_4, in.	e_5, in.	e_6, in.	g_1, in.	g_2, in.	h, in.	E, lb/in^4	ρ, lb-sec^2/in^4
1	Aluminum	6.02	4.02	0.60	3.01	1.00	2.02	3.04	0.83	1.85	2.84			0.050	10.5×10^6	0.2617×10^{-3}
2	Titanium	6.03	3.00	.60	3.01	.76	1.51	2.27	.57	1.33	2.11	3.75	1.5	.044	15.0	.4042
3	Aluminum	3.97	3.02	.40	2.00	.75	1.52	2.28	.67	1.35	2.12			.032	10.5	.2617
4	Steel	4.08	3.00	.40	2.04	.76	1.50	2.26	.59	1.34	2.07			.032	30.0	.8084
5	Steel	4.00	2.97	.40	2.00	.75	1.50	2.25	.57	1.32	2.06			.093	30.0	.8084
6	Titanium	6.03	3.01	1.50	3.51	.75	1.50	2.26	.56	1.30	2.08			.044	15.0	.4042
7	Steel	6.04	4.01	.61	3.01	1.01	2.01	3.03	.81	1.82	2.85			.050	30.0	.8084
8	Aluminum	4.03	3.02	.44	2.04	.76	1.52	2.27	.59	1.34	2.08			.093	10.5	.2617

(b) Clamped-free-clamped-free panels (see fig. 3(b))

Panel	Material	a, in.	b, in.	c, in.	d, in.	e_1, in.	e_2, in.	e_3, in.	g, in.	h, in.	E, lb/in^4	ρ, lb-sec^2/in^4
1	Titanium	6.06	3.00	0.56	3.00	1.50	0.50	2.50	5.50	0.050	15.0×10^6	0.4060×10^{-3}
2	Steel	6.10	3.00	.50	3.00	1.50	.50	2.50	5.50	.032	30.0	.7400
3	Aluminum	6.06	3.00	.55	3.00	1.50	.50	2.50	5.48	.032	10.5	.2500

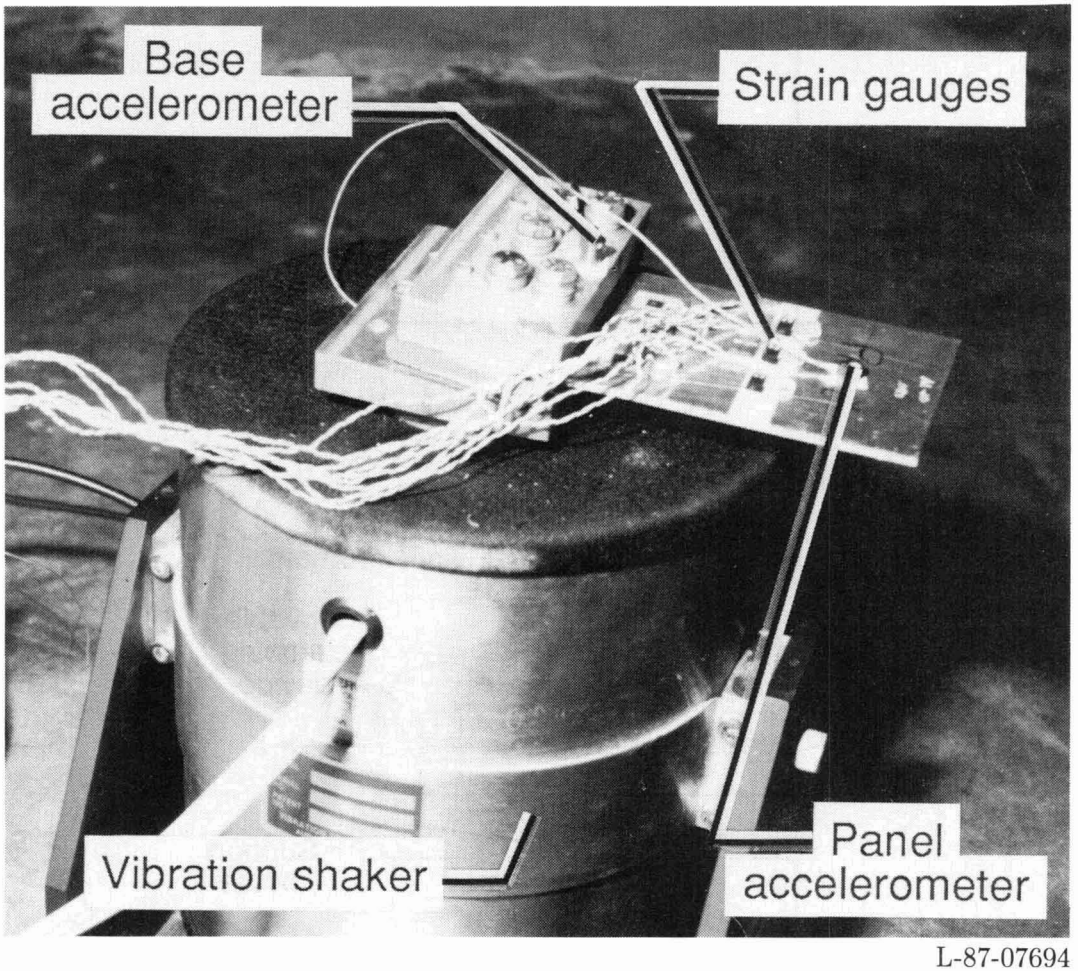

L-87-07694

Figure 1. Photograph of cantilevered test apparatus.

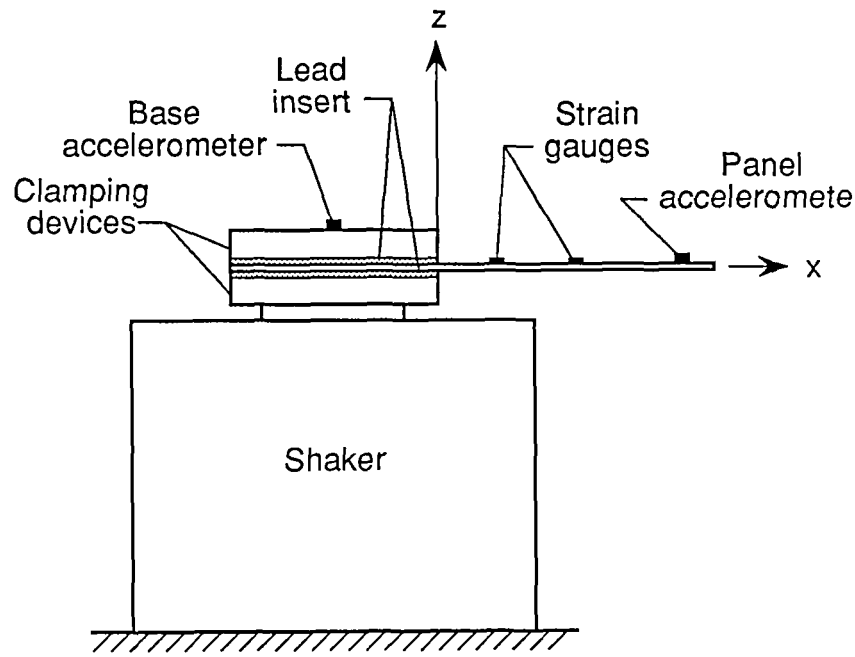

(a) Cantilevered apparatus.

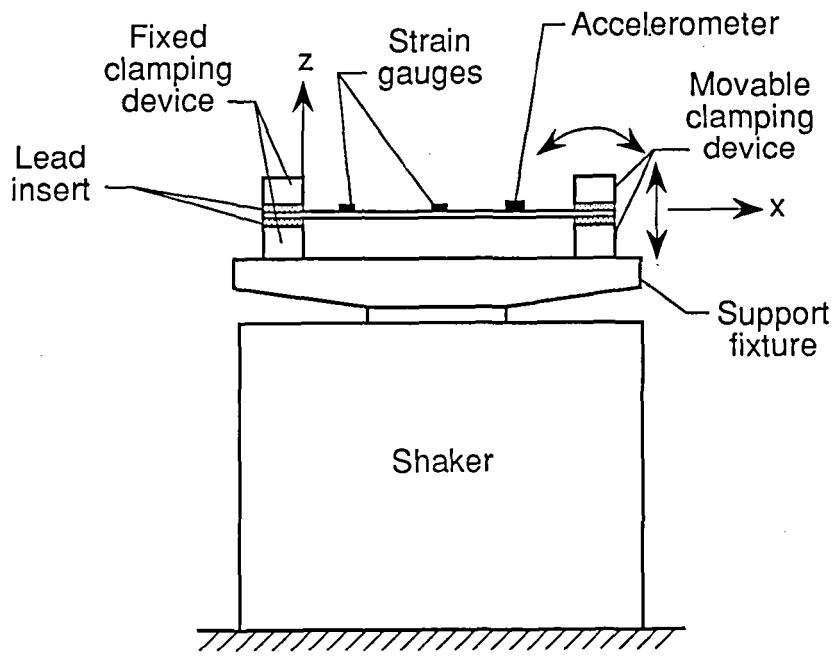

(b) Clamped-free-clamped-free apparatus.

Figure 2. Sketches of test apparatus used.

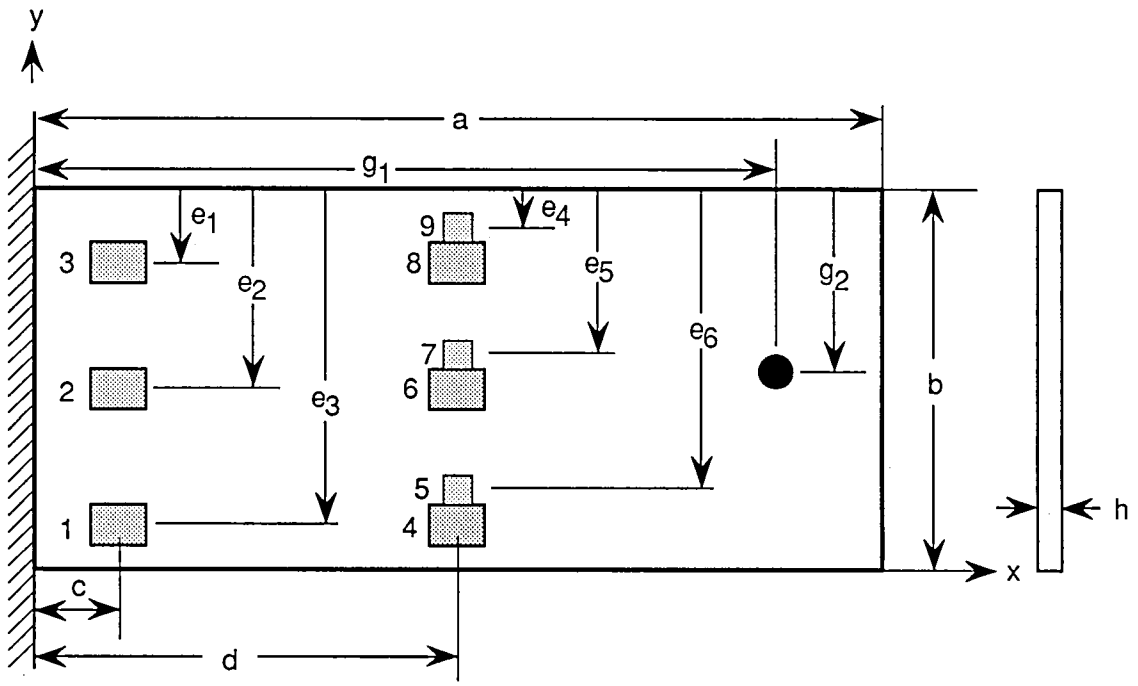

(a) Cantilevered panels. (See table I(a).)

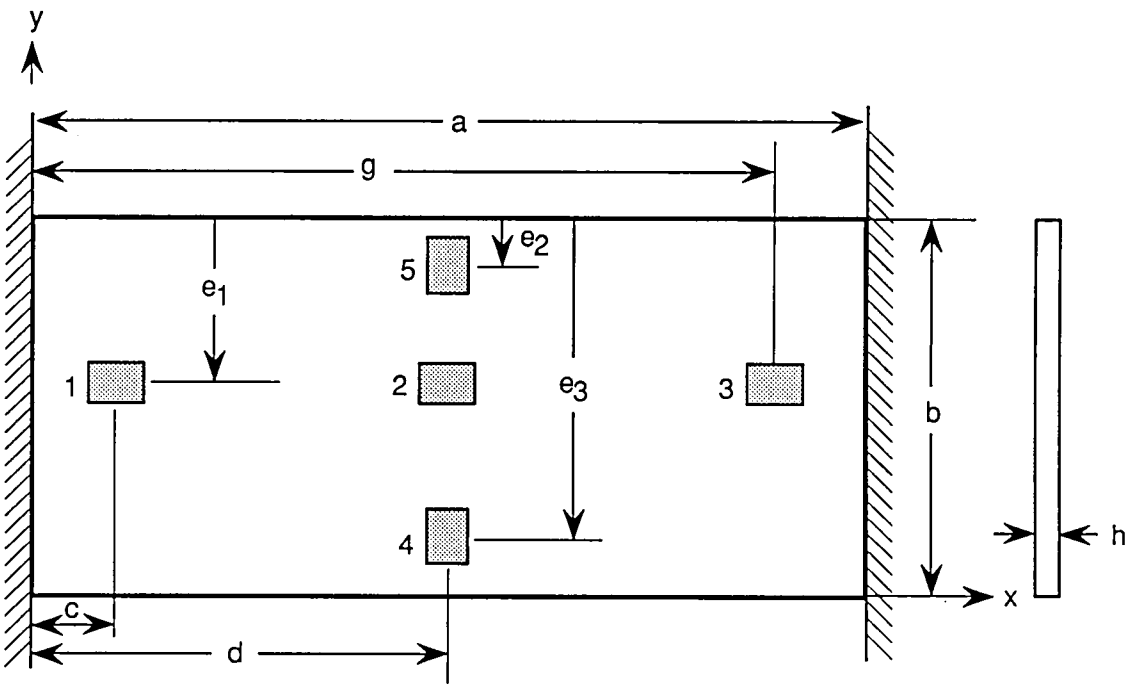

(b) Clamped-free-clamped-free panels. (See table I(b).)

Figure 3. Transducer locations.

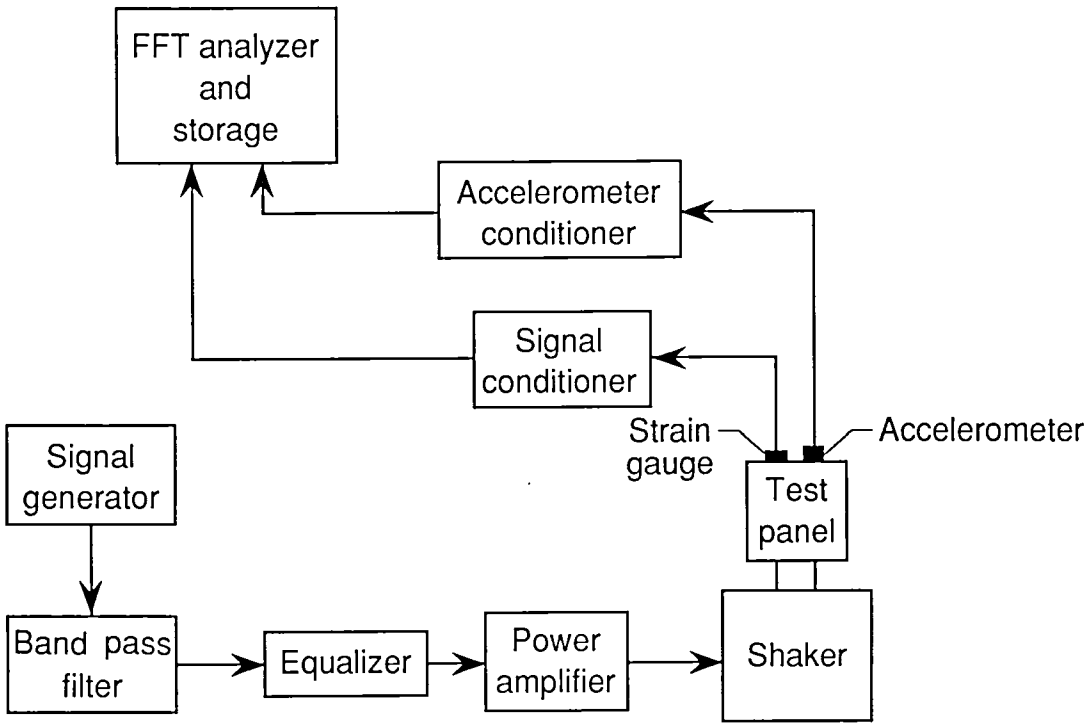

Figure 4. Diagram of instrumentation setup.

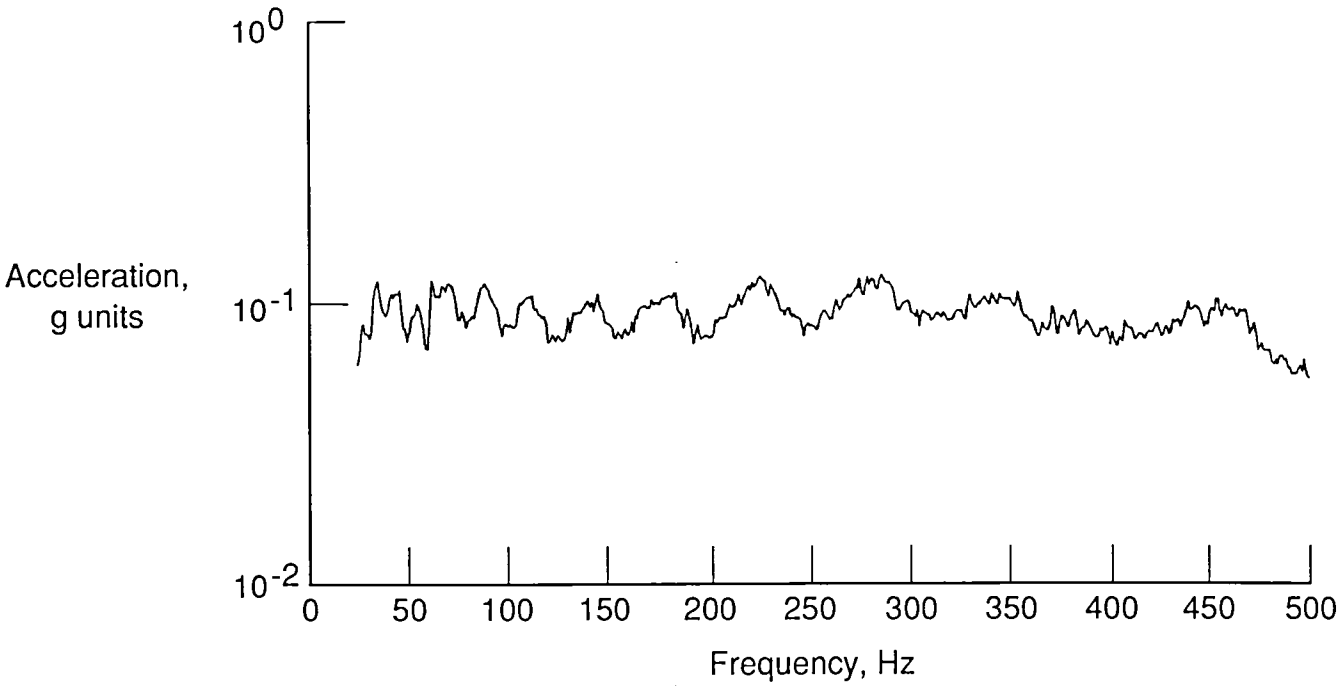

Figure 5. Sample base acceleration for cantilevered panel 4.

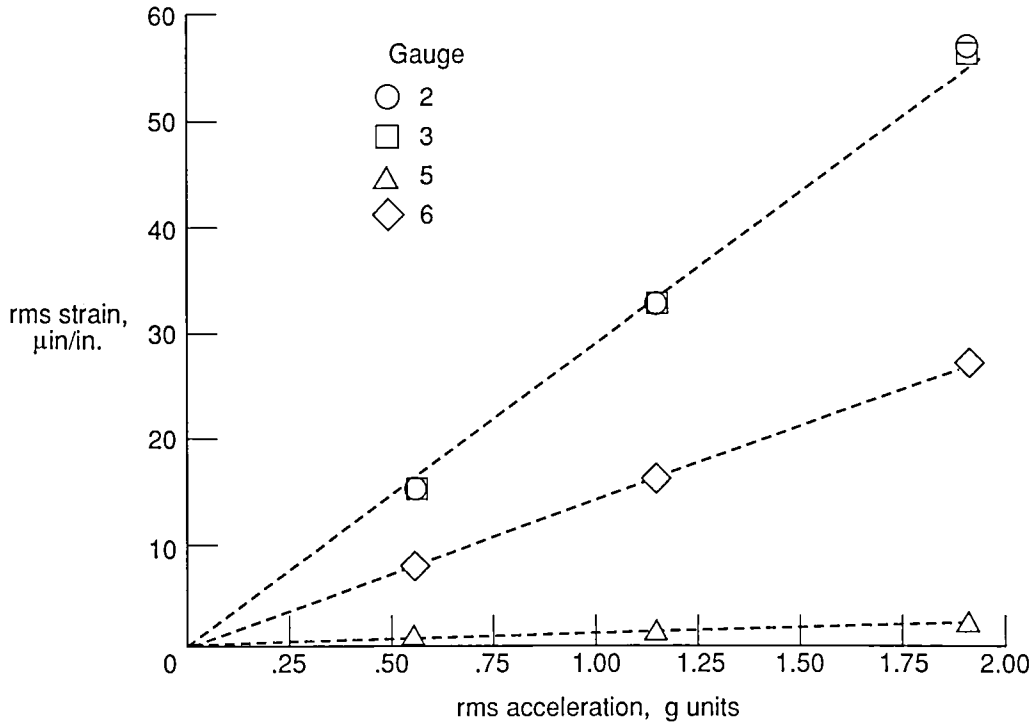

Figure 6. Relationship of rms microstrain base acceleration for cantilevered panel 4.

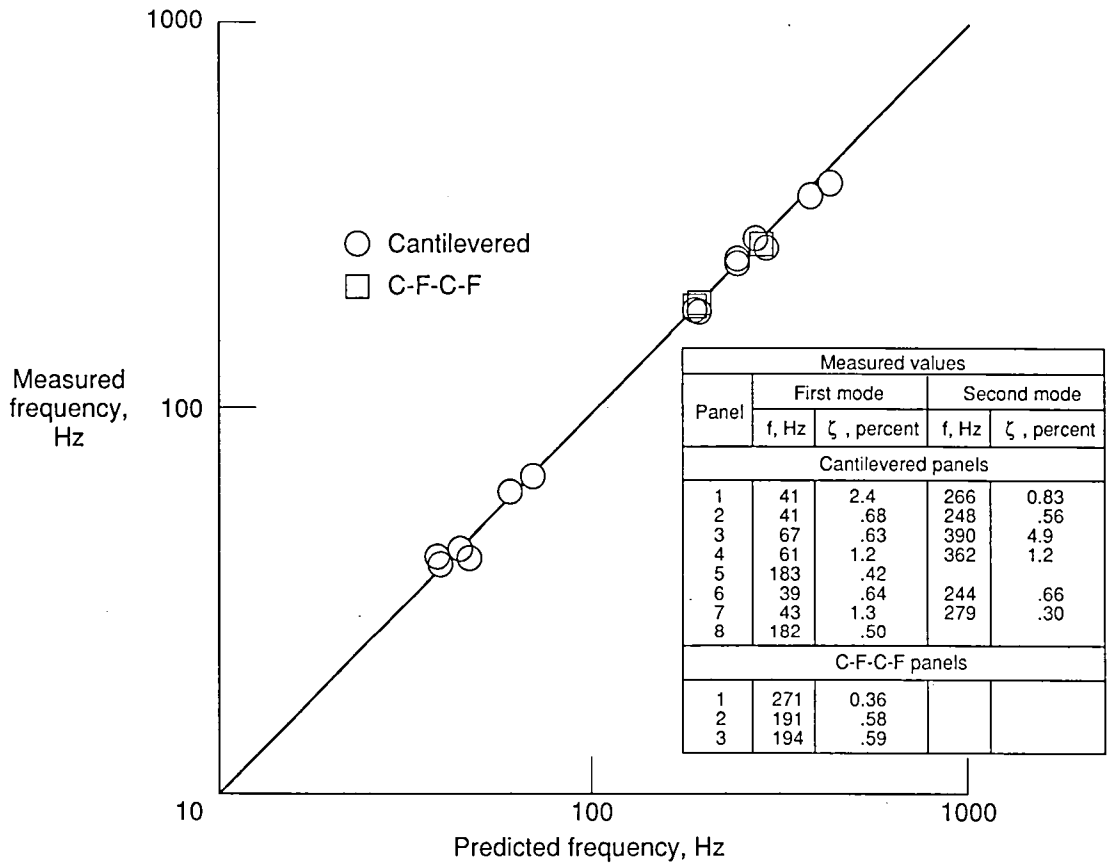

Measured values				
Panel	First mode		Second mode	
	f, Hz	ζ, percent	f, Hz	ζ, percent
Cantilevered panels				
1	41	2.4	266	0.83
2	41	.68	248	.56
3	67	.63	390	4.9
4	61	1.2	362	1.2
5	183	.42		
6	39	.64	244	.66
7	43	1.3	279	.30
8	182	.50		
C-F-C-F panels				
1	271	0.36		
2	191	.58		
3	194	.59		

Figure 7. Measured and predicted natural frequencies for cantilevered and C-F-C-F panels.

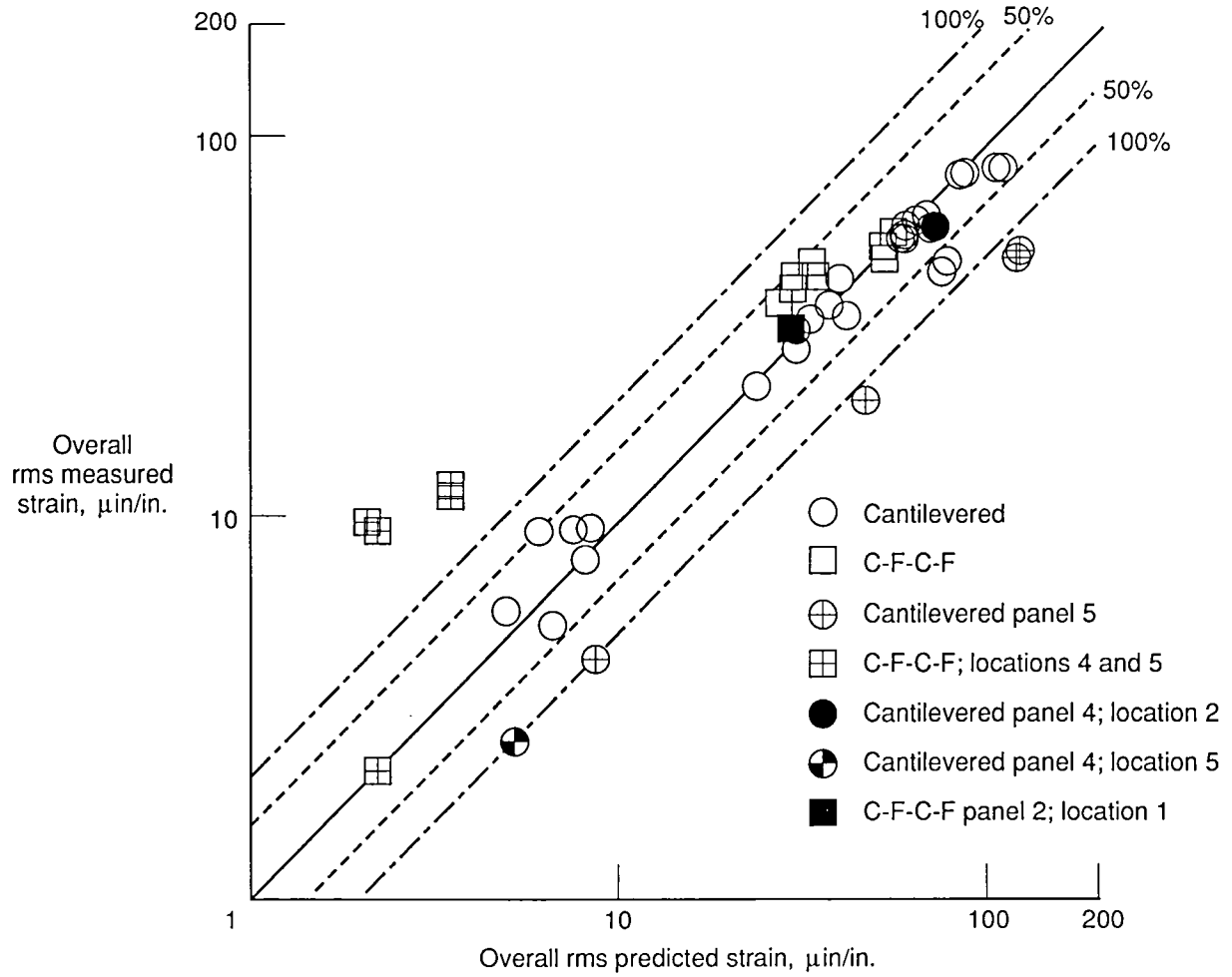

Figure 8. Measured and predicted overall rms strains for cantilevered and C-F-C-F panels (eqs. (31)).

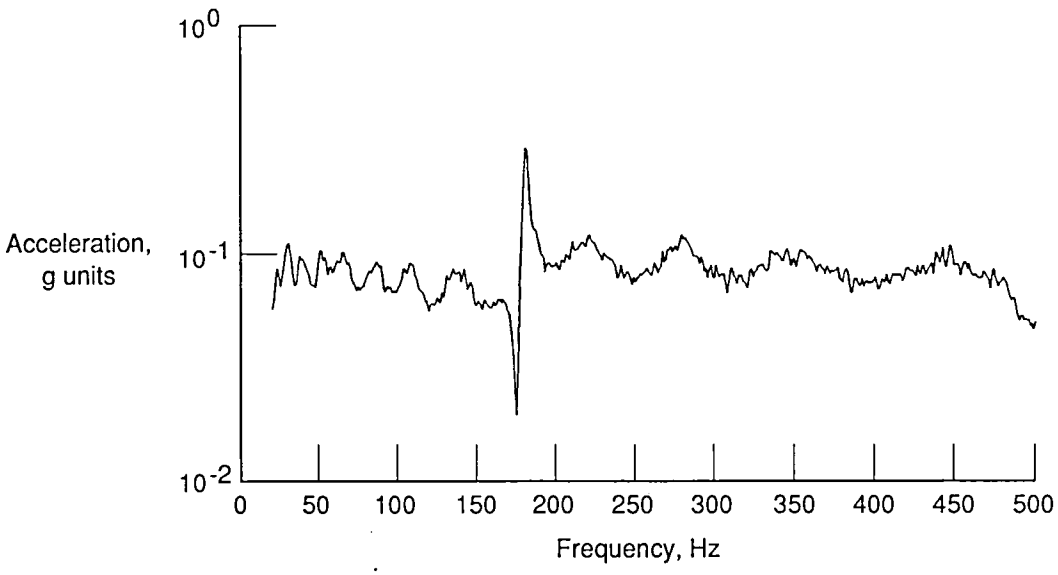

Figure 9. Base acceleration for cantilevered panel 5.

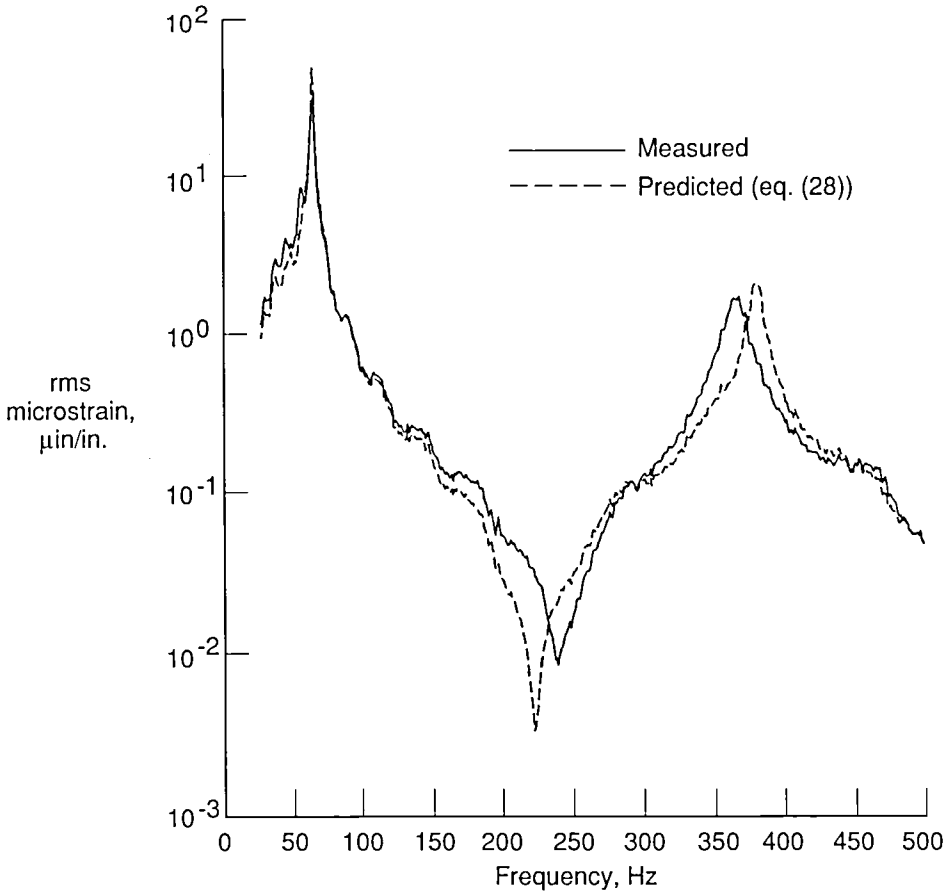

Figure 10. Measured and predicted strain spectra for location 2 on cantilevered panel 4.

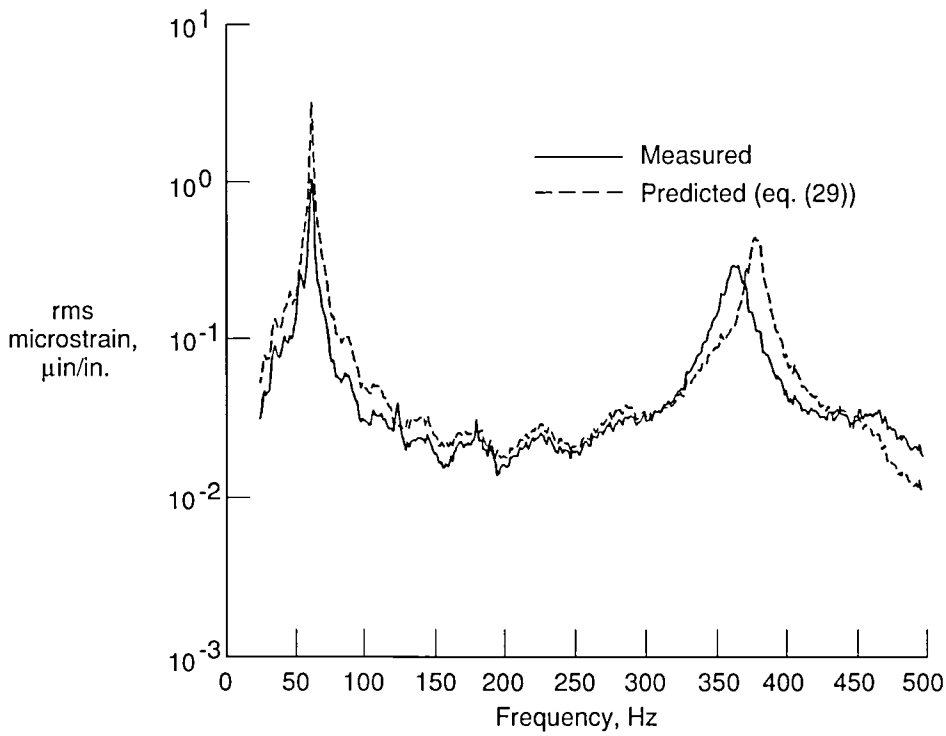

Figure 11. Measured and predicted strain spectra for location 5 on cantilevered panel 4.

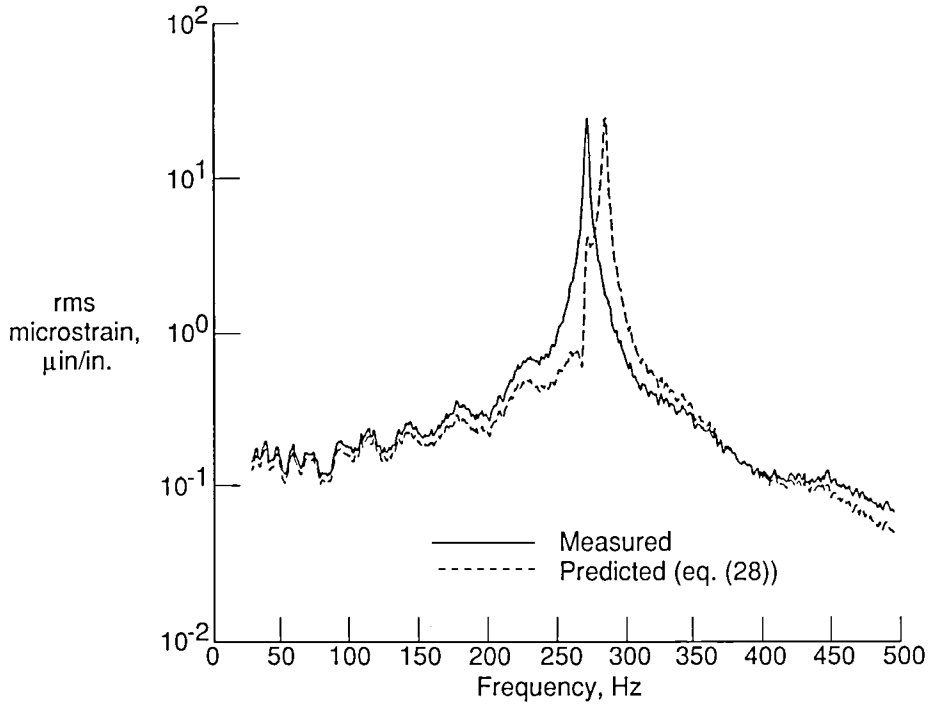

Figure 12. Measured and predicted strain spectra for location 1 on C-F-C-F panel 2.

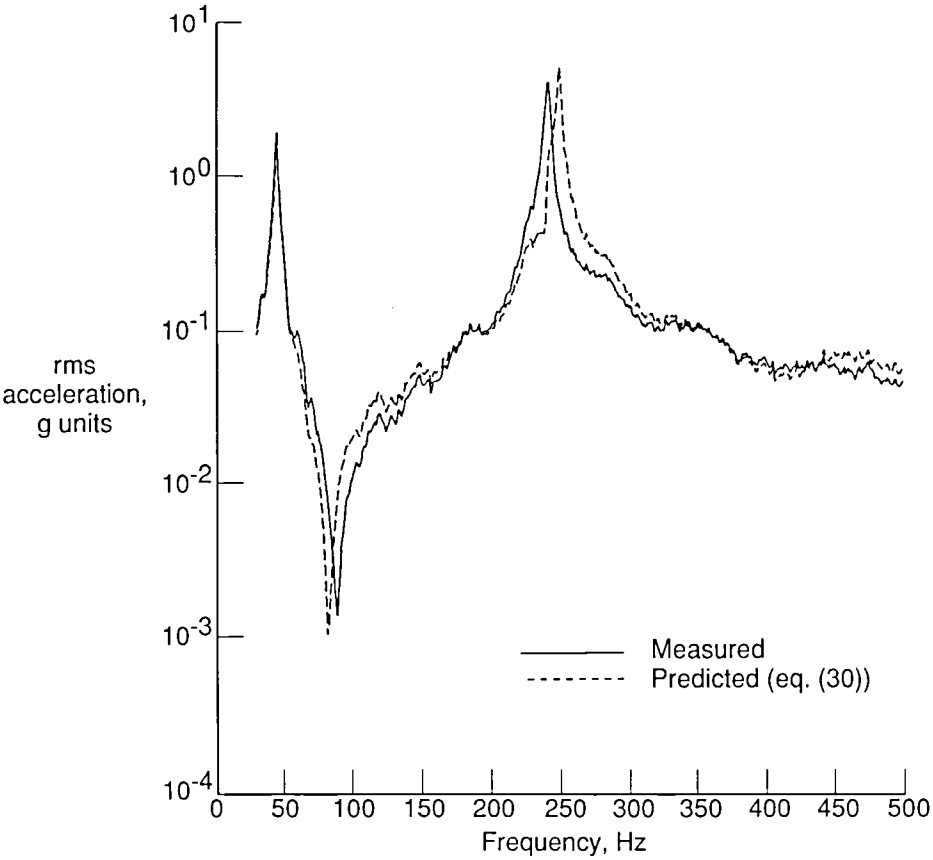

Figure 13. Measured and predicted acceleration spectra for cantilevered panel 2.

NASA
National Aeronautics and Space Administration

Report Documentation Page

1. Report No.	2. Government Accession No.	3. Recipient's Catalog No.
NASA TM-4054 AVSCOM TM-88-B-013		

4. Title and Subtitle
Predicted and Measured Strain Responses of Isotropic Panels to Base Excitation

5. Report Date
August 1988

6. Performing Organization Code

7. Author(s)
Karen H. Lyle, Jack D. Leatherwood, and Edward F. Daniels

8. Performing Organization Report No.
L-16446

9. Performing Organization Name and Address
Aerostructures Directorate
USAARTA–AVSCOM
Langley Research Center
Hampton, VA 23665-5225
and
NASA Langley Research Center
Hampton, VA 23665-5225

10. Work Unit No.
506-80-31-02

11. Contract or Grant No.

12. Sponsoring Agency Name and Address
National Aeronautics and Space Administration
Washington, DC 20546-0001
and
U.S. Army Aviation Systems Command
St. Louis, MO 63120-1798

13. Type of Report and Period Covered
Technical Memorandum

14. Army Project No.
1L161102AH45C

15. Supplementary Notes
Karen H. Lyle: Aerostructures Directorate, USAARTA–AVSCOM, Hampton, Virginia.
Jack D. Leatherwood and Edward F. Daniels: Langley Research Center, Hampton, Virginia.

16. Abstract

The objective of the research described is to assess the accuracy of classical linear theory for predicting acceleration and strain for cantilevered and clamped-free-clamped-free (C-F-C-F) panels excited through the base. Aluminum, stainless steel, and titanium panels of various dimensions and thicknesses were vibration tested by using a broadband random signal applied through a shaker mounting fixture. The strains were measured at nine locations on each cantilevered panel and at five locations on each C-F-C-F panel. Accelerations were measured on the base and at one panel location for both the cantilevered and the C-F-C-F panels. Predictions were based on the Ritz method. The measured accelerations of the base were input to the analysis for the forcing function. Comparisons between predicted and measured strain and acceleration spectra were within an average error of 20 percent for both the cantilevered and the C-F-C-F panels.

17. Key Words (Suggested by Authors(s))	18. Distribution Statement
Ritz method Structural strain Strain measurement Rectangular panels	Unclassified—Unlimited Subject Category 39

19. Security Classif.(of this report)	20. Security Classif.(of this page)	21. No. of Pages	22. Price
Unclassified	Unclassified	21	A02

NASA FORM 1626 OCT 86
NASA-Langley, 1988
For sale by the National Technical Information Service, Springfield, Virginia 22161-2171

National Aeronautics and
Space Administration
Code NTT-4

Washington, D.C.
20546-0001